

Search for Muon Neutrino and Antineutrino Disappearance in MiniBooNE

A. A. Aguilar-Arevalo,¹⁴ C. E. Anderson,¹⁹ A. O. Bazarko,¹⁶ S. J. Brice,⁷ B. C. Brown,⁷ L. Bugel,⁵ J. Cao,¹⁵ L. Coney,⁵ J. M. Conrad,^{5,13} D. C. Cox,¹⁰ A. Curioni,¹⁹ Z. Djurcic,⁵ D. A. Finley,⁷ B. T. Fleming,¹⁹ R. Ford,⁷ F. G. Garcia,⁷ G. T. Garvey,¹¹ J. Grange,⁸ C. Green,^{7,11} J. A. Green,^{10,11} T. L. Hart,⁴ E. Hawker,^{3,11} R. Imlay,¹² R. A. Johnson,³ G. Karagiorgi,^{5,13} P. Kasper,⁷ T. Katori,^{10,13} T. Kobilarcik,⁷ I. Kourbanis,⁷ S. Koutsoliotas,² E. M. Laird,¹⁶ S. K. Linden,¹⁹ J. M. Link,¹⁸ Y. Liu,¹⁵ Y. Liu,¹ W. C. Louis,¹¹ K. B. M. Mahn,⁵ W. Marsh,⁷ C. Mauger,¹¹ V. T. McGary,^{5,13} G. McGregor,¹¹ W. Metcalf,¹² P. D. Meyers,¹⁶ F. Mills,⁷ G. B. Mills,¹¹ J. Monroe,⁵ C. D. Moore,⁷ J. Mousseau,⁸ R. H. Nelson,⁴ P. Nienaber,¹⁷ J. A. Nowak,¹² B. Osmanov,⁸ S. Ouedraogo,¹² R. B. Patterson,¹⁶ Z. Pavlovic,¹⁶ D. Perevalov,¹ C. C. Polly,^{9,10} E. Prebys,⁷ J. L. Raaf,³ H. Ray,^{8,11} B. P. Roe,¹⁵ A. D. Russell,⁷ V. Sandberg,¹¹ R. Schirato,¹¹ D. Schmitz,⁵ M. H. Shaevitz,⁵ F. C. Shoemaker,^{16,*} D. Smith,⁶ M. Soderberg,¹⁹ M. Sorel,^{5,†} P. Spentzouris,⁷ J. Spitz,¹⁹ I. Stancu,¹ R. J. Stefanski,⁷ M. Sung,¹² H. A. Tanaka,¹⁶ R. Tayloe,¹⁰ M. Tzanov,⁴ R. G. Van de Water,¹¹ M. O. Wascko,^{12,‡} D. H. White,¹¹ M. J. Wilking,⁴ H. J. Yang,¹⁵ G. P. Zeller,^{5,11} and E. D. Zimmerman⁴

(MiniBooNE Collaboration)

¹University of Alabama, Tuscaloosa, Alabama 35487, USA

²Bucknell University, Lewisburg, Pennsylvania 17837, USA

³University of Cincinnati, Cincinnati, Ohio 45221, USA

⁴University of Colorado, Boulder, Colorado 80309, USA

⁵Columbia University, New York, New York 10027, USA

⁶Embry Riddle Aeronautical University, Prescott, Arizona 86301, USA

⁷Fermi National Accelerator Laboratory, Batavia, Illinois 60510, USA

⁸University of Florida, Gainesville, Florida 32611, USA

⁹University of Illinois, Urbana, Illinois 61801, USA

¹⁰Indiana University, Bloomington, Indiana 47405, USA

¹¹Los Alamos National Laboratory, Los Alamos, New Mexico 87545, USA

¹²Louisiana State University, Baton Rouge, Louisiana 70803, USA

¹³Massachusetts Institute of Technology, Cambridge, Massachusetts 02139, USA

¹⁴Universidad Nacional Autonoma de Mexico, Mexico, Distrito Federal, Mexico

¹⁵University of Michigan, Ann Arbor, Michigan 48109, USA

¹⁶Princeton University, Princeton, New Jersey 08544, USA

¹⁷Saint Mary's University of Minnesota, Winona, Minnesota 55987, USA

¹⁸Virginia Polytechnic Institute and State University, Blacksburg, Virginia 24061, USA

¹⁹Yale University, New Haven, Connecticut 06520, USA

(Received 11 March 2009; published 4 August 2009)

The MiniBooNE Collaboration reports a search for ν_μ and $\bar{\nu}_\mu$ disappearance in the Δm^2 region of 0.5–40 eV². These measurements are important for constraining models with extra types of neutrinos, extra dimensions, and *CPT* violation. Fits to the shape of the ν_μ and $\bar{\nu}_\mu$ energy spectra reveal no evidence for disappearance at the 90% confidence level (C.L.) in either mode. The test of $\bar{\nu}_\mu$ disappearance probes a region below $\Delta m^2 = 40$ eV² never explored before.

DOI: 10.1103/PhysRevLett.103.061802

PACS numbers: 14.60.St, 14.60.Lm, 14.60.Pq

Neutrino oscillations have been observed and confirmed at mass splittings (Δm^2) of $\sim 10^{-5}$ eV² and $\sim 10^{-3}$ eV², called the “solar” and “atmospheric” oscillations, respectively. The observed mixing is consistent with three generations of neutrinos and a unitary mixing matrix. Complicating this picture, the Liquid Scintillator Neutrino Detector (LSND) experiment observed an excess of $\bar{\nu}_e$ in a $\bar{\nu}_\mu$ beam [1], indicating a possible third Δm^2 around 1 eV² thus requiring more than three neutrino generations or other exotic physics. Recently, the MiniBooNE experiment [2] excluded two-neutrino

appearance-only oscillations (98% C.L.) as an explanation of the LSND excess if oscillations of neutrinos and anti-neutrinos are the same.

Exotic physics models [3–6], including sterile neutrinos, extra dimensions, and *CPT* violation, have been proposed to explain the LSND observation. Some of these models can also accommodate the MiniBooNE ν_e appearance oscillation results. These models are testable with measurements of ν_μ and $\bar{\nu}_\mu$ disappearance which constrain any nonstandard oscillations of $\bar{\nu}_\mu \rightarrow \bar{\nu}_x$. As described in this Letter, the MiniBooNE Collaboration has performed

searches for ν_μ and $\bar{\nu}_\mu$ disappearance which probe a region of interest, $\Delta m^2 = 0.5\text{--}40\text{ eV}^2$, not covered by two previous disappearance experiments, CCFR (ν_μ and $\bar{\nu}_\mu$) [7] and CDHS (ν_μ only) [8]. Unless otherwise stated, all statements about neutrinos hold true also for antineutrinos.

For the MiniBooNE experimental setup, the detector [9] is located at a fixed distance from the neutrino source. In this case, ν_μ disappearance due to oscillations has a distinct signature as a function of neutrino energy, because neutrinos with different energies oscillate with different probabilities for the same distance traveled. Disappearance would be observable either via a deficit of events (normalization) or, alternatively, via a distortion of the neutrino energy spectrum (shape), or both (normalization + shape). The absolute normalization uncertainties in a single detector experiment such as MiniBooNE are large, so a shape-only disappearance fit is performed. The $(\bar{\nu}_\mu^-)$ flux to the MiniBooNE detector is provided by the Fermilab Booster Neutrino Beam, produced by 8 GeV protons incident on a 1 cm diameter, 71 cm long (1.7 interaction length) beryllium target surrounded by a magnetic horn pulsed at 174 kA. The horn uses a positive current to focus π^+ and K^+ mesons for the neutrino mode sample, and a negative current to focus π^- and K^- for the antineutrino mode sample. The mesons that pass through a 60 cm diameter collimator 259 cm downstream of the target decay in a 50 m long tunnel to produce the $(\bar{\nu}_\mu^-)$ beam. The Booster Neutrino Beam flux [10] is determined using a GEANT4 [11] based beam simulation which has been further modified to include updated p -Be particle production data [12,13].

The distance from the proton interaction target to the MiniBooNE detector [9] is 541 m. The MiniBooNE detector is a 12 m diameter spherical tank filled with 800 tons of mineral oil (CH_2). The detector is separated into an inner region filled with 1280 inward-facing 8 in. photomultiplier tubes (PMTs), and an optically isolated outer region used to reject cosmic-ray induced events. Charged particles produced in neutrino interactions emit primarily Cherenkov light, though a small amount of scintillation light is also produced. Light and particle production and propagation in the MiniBooNE detector is modeled using a GEANT3 [14] based simulation, which was tuned using MiniBooNE and external data.

Neutrino interactions are simulated with the v3 NUANCE event generator [15]. Prior to selection, approximately 42% of all events in MiniBooNE are charged current quasielastic (CCQE) scattering, and 22% are charged current single charged pion production ($\text{CC1 } \pi^{+/-}$) in both the neutrino and antineutrino mode.

The search for oscillations is conducted with a sample of CCQE events because of the high statistics and purity. The

reconstructed neutrino energy (E_ν^{QE}) is calculated assuming the target nucleon is at rest:

$$E_\nu^{\text{QE}} = \frac{2(M_n - E_B)E_\mu - (E_B^2 - 2M_n E_B + \Delta M + M_\mu^2)}{2[(M_n - E_B) - E_\mu + p_\mu \cos\theta_\mu]}, \quad (1)$$

where $\Delta M = M_n^2 - M_p^2$; M indicates the muon, proton, or neutron mass with appropriate subscripts; E_B is the nucleon binding energy; $E_\mu(p_\mu)$ is the reconstructed muon energy (momentum); and θ_μ is the reconstructed muon scattering angle with respect to the neutrino beam direction. A small correction is applied in both data and simulation to account for the biasing effects of Fermi smearing. At 300 MeV, the muon energy resolution is 7% and the angular resolution is 5 degrees. The average E_ν^{QE} resolution is 11% for CCQE events [16].

A CCQE event sample is selected by identifying a single muon in the detector and its associated decay electron, using the same criteria as in the previous measurement of CCQE model parameters on carbon [16]. Timing information from the PMTs allows the light produced by the initial neutrino interaction (first ‘‘subevent’’) to be separated from the light produced by the decay electron (second subevent). The timing and charge response of the PMTs is then used to reconstruct the position, kinetic energy, and direction vector of the primary particle within each subevent. Exactly two subevents are required in the analysis (the muon and its decay electron). Requiring both subevents to have fewer than six PMT hits anywhere in the veto region rejects 99.99% of all cosmic-ray interactions [9]. The first subevent must be in coincidence with a beam pulse, and have greater than 200 inner tank PMT hits, to eliminate electrons from stopped cosmic-ray muon decays. The mean emission point of the Cherenkov light along the track for the first subevent must be less than 500 cm from the center of the tank. The second subevent must have fewer than 200 inner PMT hits to be consistent with the decay electron energy endpoint. Finally, the distance between the electron vertex and the muon track endpoint must be less than 100 cm, ensuring that the electron is associated with the muon track. This selection also applies to the antineutrino mode sample, as the final state nucleon is not reconstructed and the detector does not distinguish muon charge.

The selection criteria yield 190 454 data events with $0 < E_\nu^{\text{QE}} < 1.9\text{ GeV}$ for 5.58×10^{20} protons on target in the neutrino mode sample, and 27 053 data events for 3.39×10^{20} protons on target in the antineutrino mode sample. According to the simulation, the neutrino mode sample is 74% pure CCQE, and the antineutrino mode sample is 70% pure CCQE. The primary background ($\sim 75\%$) for both the ν_μ and $\bar{\nu}_\mu$ samples is $\text{CC1 } \pi$ events where the outgoing pion is unobserved (due, e.g., to absorption in the nucleus). Though the neutrino mode sample has $< 1\%$ $\bar{\nu}_\mu$ content, the

beam in the antineutrino mode contains a substantial contribution of ν_μ due to the higher π^+ production at the target and the higher ν_μ cross section. The antineutrino mode is predicted to have 25% ν_μ content.

The CCQE cross section depends on the axial vector form factor, which is commonly assumed to have a dipole form as a function of four-momentum transfer (Q^2) with one adjustable parameter, M_A , the axial mass. Global fits to the world's neutrino scattering data on deuterium yield $M_A = 1.015$ GeV [17]. However, recent results from K2K ($M_A = 1.14 \pm 0.11$ GeV, on carbon [18]; $M_A = 1.20 \pm 0.12$ GeV, on oxygen [19]) and MiniBooNE ($M_A = 1.23 \pm 0.12$ GeV, on carbon [16]) suggest a higher effective value of M_A for nuclear targets. In addition, the level of Pauli blocking was adjusted in the MiniBooNE analysis, using a parameter $\kappa = 1.019$, to better reproduce the experimental data at low Q^2 [16]. The effect of M_A and κ on the Q^2 shape is pronounced, but oscillations would provide relatively little Q^2 distortion; this means that a spurious value of M_A or κ cannot be caused by underlying oscillations. The MiniBooNE CCQE ν_μ analysis which produced a value of $M_A = 1.23$ assumed no oscillations, and therefore those values of M_A and κ should not be used in a disappearance analysis of the same data set. Consequently, the lower values of M_A and κ are used with conservative uncertainties which span the difference between the deuterium and nuclear target results ($M_A = 1.015 \pm 0.20$ GeV, $\kappa = 1.000 \pm 0.019$). The disappearance limits obtained were insensitive to the values of M_A and κ used. With $M_A = 1.015$ GeV and $\kappa = 1.000$, the ratio of detected events to predicted events in MiniBooNE is 1.31 ± 0.26 for neutrinos and 1.18 ± 0.18 for antineutrinos. The ratio for neutrinos reported in Ref. [16] is lower because higher values of M_A and κ were used there.

For the disappearance search, systematic uncertainties are included for the underlying neutrino flux prediction, neutrino interaction cross section, and detector response. The method used to estimate the uncertainties due to the underlying neutrino flux prediction and detector model is identical to the method used in previous MiniBooNE results [2,20]. The uncertainties on the cross section include uncertainties on the CCQE cross section and CC1 π background. The latter is estimated using the MiniBooNE CC1 π^+ data sample. Systematic uncertainties produce correlated errors between E_ν^{QE} bins that are included by developing a covariance matrix in the same manner as in previous MiniBooNE oscillation analyses [2,20]. This covariance matrix includes separate normalization and shape-only error contributions. For the shape-only disappearance search, the prediction is normalized to data, and just the shape-only covariance matrix is used.

The disappearance search uses the Pearson's χ^2 test to determine allowed regions in the $\Delta m^2 - \sin^2 2\theta$ plane. The χ^2 is calculated from a comparison of the data, d_i , in the E_ν^{QE} bin i , to a prediction $p_i(\Delta m^2, \sin^2 2\theta)$ for 16 bins. The

prediction assumes a two-flavor $\nu_\mu \rightarrow \nu_x$ disappearance characterized by one large mass splitting ($\Delta m^2 \equiv \Delta m_{hk}^2$) between the light neutrino mass states k , which participate in standard three-neutrino oscillations, and h , the heavier neutrino state, and one oscillation amplitude $\sin^2 2\theta = 4|U_{\mu,h}|^2(1 - |U_{\mu,h}|^2)$, where $|U_{\mu,h}|^2$ is the muon flavor content of the heavy state h :

$$\chi^2 = \sum_{i,j}^{16 \text{ bins}} (d_i - N p_i) M_{ij}^{-1} (d_j - N p_j), \quad (2)$$

where M_{ij} is the shape-only error matrix, and N is a factor which normalizes the prediction to the total number of observed events in data. All neutrino events in the prediction, including the CC1 π^+ background events, are allowed to oscillate in the fit based on the incident neutrino energy and distance traveled. The 90% C.L. limit corresponds to $\chi^2 > 23.5$ for 16 degrees of freedom (DF). The sensitivity is a fit to an unoscillated prediction including all statistical and systematic uncertainties.

The top plot of Fig. 1 (Fig. 2) shows the E_ν^{QE} spectrum after selection cuts for the neutrino (antineutrino) data and

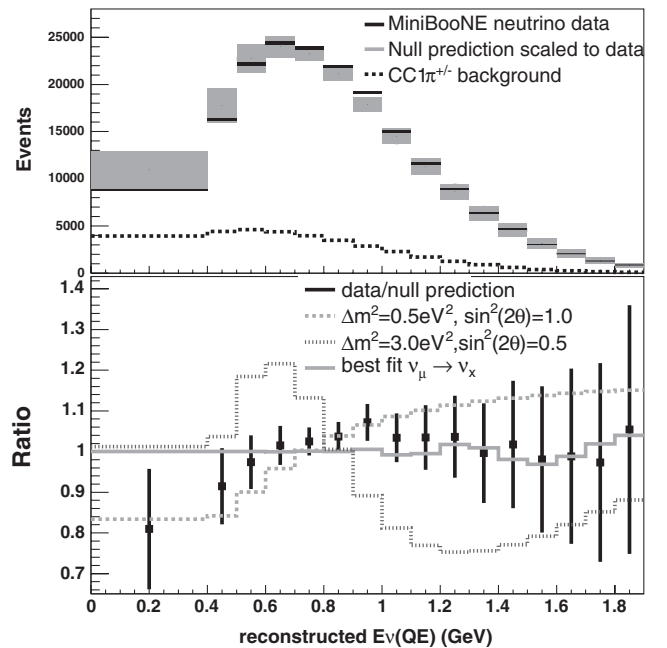


FIG. 1. The top plot shows the E_ν^{QE} distribution for neutrino data (black) with statistical error rectangles (thickness of line indicates size of statistical error), and the prediction assuming no oscillations [area normalized to number of data events (grey)]. Attached to the prediction are the diagonal elements of the shape error matrix. The predicted CC1 π background (dashed line) events are also shown. The background antineutrino events are negligible. The bottom plot shows the ratio of data to no oscillations (black solid line), and the ratio of no oscillations to $\Delta m^2 = 0.5$ eV², $\sin^2 2\theta = 1.0$ disappearance (dashed line), $\Delta m^2 = 3.0$ eV², $\sin^2 2\theta = 0.5$ disappearance (dotted line), and for the minimum $\chi^2 = 12.72$ (13 DF) at $\Delta m^2 = 17.5$ eV², $\sin^2 2\theta = 0.16$ (solid grey line).

the prediction, assuming no oscillations (null hypothesis) with diagonal elements of the error matrix. The dominant systematics arise from the neutrino flux (production of $\pi^{+/-}$ from p -Be interactions) and CCQE cross section uncertainties; uncertainties at low energy are larger because of the substantial CC1 π^+ background and uncertainties in the CCQE cross section in this region. As shown in Fig. 1, the individual bin errors are large, but adjacent bins are nearly fully correlated. The χ^2 between the data and the null hypothesis is 17.78 (16 DF, 34% probability) for the neutrino mode sample, which is consistent with no oscillations at the 90% C.L. The top plot of Fig. 3 shows the 90% C.L. sensitivity and limit curves for the neutrino mode sample. The minimum $\chi^2 = 12.72$ (13 DF, 47% probability) at $\Delta m^2 = 17.5 \text{ eV}^2$, $\sin^2 2\theta = 0.16$. The probability distribution and number of degrees of freedom for the χ^2 statistic are determined from an analysis of a set of simulated data samples, as suggested in Ref. [21].

The bottom plot in Fig. 1 shows the ratio of data to the null hypothesis and three oscillation scenarios. The shape distortion for $\Delta m^2 = 0.5 \text{ eV}^2$ is very different from $\Delta m^2 = 3.0 \text{ eV}^2$. The χ^2 therefore changes rapidly as a function of Δm^2 , resulting in rapid changes in the 90% C.L. sensitivity and limit curves (Fig. 3) for small differences in Δm^2 . Similar features are also seen in previous disappearance analyses [7,8].

The $\bar{\nu}_\mu$ disappearance analysis proceeds in the same manner as the ν_μ analysis, except that only the $\bar{\nu}_\mu$ events are allowed to oscillate in the fit and the ν_μ events are kept

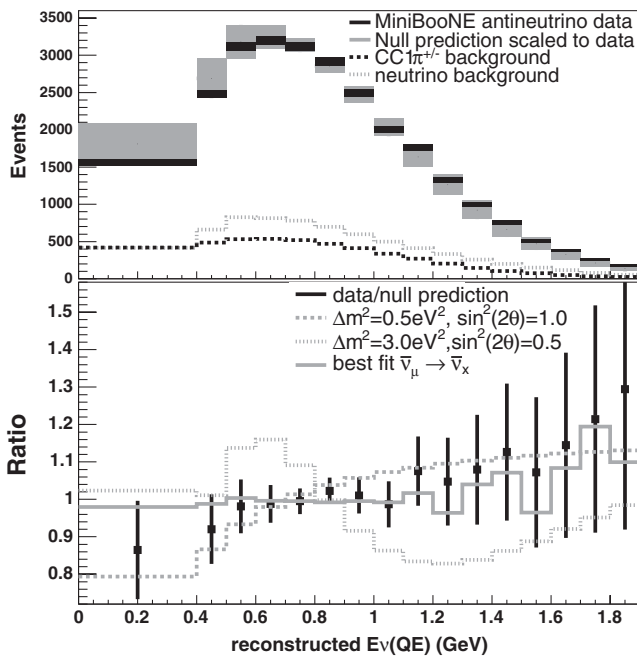


FIG. 2. Same convention as Fig. 1 for the antineutrino mode sample. The background neutrino events are also shown (dotted line in top plot). Minimum $\chi^2 = 5.43$ (11 DF) is at $\Delta m^2 = 31.3 \text{ eV}^2$, $\sin^2 2\theta = 0.96$.

fixed. This determines the limit on a model where the $\bar{\nu}_\mu$ can oscillate but the ν_μ cannot. A model where both ν_μ and $\bar{\nu}_\mu$ oscillate with equal oscillation probability versus energy would produce a limit very similar to the neutrino mode limit.

During antineutrino data taking, two absorber plates inadvertently fell vertically into the decay volume at 25 m and were later removed, creating three distinct data taking periods with zero, one, or two absorbers in the beam line. The event rate was predicted to be 13% (20%) lower for one (two) plate(s) in the beam. One (two) absorber plate (s) were in the beam for 16.8% (18.1%) of the antineutrino data taking. Beam line monitoring systems indicated when each plate dropped. Because the changes to the beam line are understood, a separate simulation was run with the appropriate number of absorber plates in the beam line. Figure 2 shows the E_ν^{QE} distribution for the antineutrino mode sample. The χ^2 of the null hypothesis is 13.7, 8.2, 15.2, 10.29 (16 DF) for the zero, one, and two absorber plate and total data, respectively. The antineutrino mode data are also consistent with no oscillations at the 90% C.L., so the bottom plot of Fig. 3 shows the 90% C.L. sensitivity and limit curves for the antineutrino disappear-

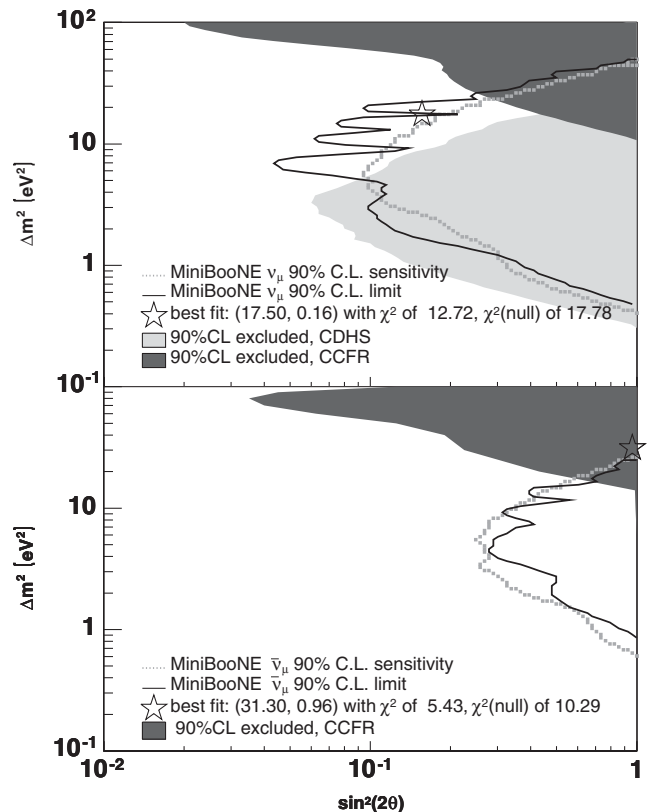


FIG. 3. The top plot shows the sensitivity (dashed line) and limit (solid line) for 90% C.L. for neutrino disappearance in MiniBooNE. Previous limits by CCFR (dark grey) and CDHS (light grey) are also shown. The bottom plot uses the same convention for antineutrino disappearance.

ance fit to all antineutrino data; the limit curves for the individual absorber data periods were found to be consistent within errors to the total.

In addition to the two-neutrino oscillation fits described above, two $3 + 2$ sterile neutrino models are tested. A $3 + 2$ model assumes two heavy neutrinos mix with the lighter neutrinos, with two mass splittings and two oscillation amplitudes. Global fits to existing appearance and disappearance data yield regions of allowed $3 + 2$ model parameters. The best fit points in these allowed regions are tested with MiniBooNE data by forming a χ^2 with a prediction assuming the full $3 + 2$ oscillation formalism with the best fit $3 + 2$ model parameters. The best fit $3 + 2$ model in Ref. [4] is consistent with both MiniBooNE ν_μ and $\bar{\nu}_\mu$ data. However, the ν_μ data are incompatible with the best fit $3 + 2$ model in Ref. [5] at the 90% C.L. with $\chi^2 = 24.7$ (16 DF).

In summary, MiniBooNE observes no evidence for ν_μ or $\bar{\nu}_\mu$ disappearance at the 90% C.L. in the Δm^2 region of 0.5–40 eV². The test of $\bar{\nu}_\mu$ disappearance probes a region unexplored by previous experiments.

We acknowledge the support of Fermilab, the Department of Energy, and the National Science Foundation. We thank Los Alamos National Laboratory for LDRD funding. We also acknowledge the use of Condor software in the analysis of the data.

*Deceased.

†Present address: IFIC, Universidad de Valencia and CSIC, Valencia 46071, Spain.

‡Present address: Imperial College, London SW7 2AZ, United Kingdom.

- [1] C. Athanassopoulos *et al.*, Phys. Rev. Lett. **75**, 2650 (1995); **77**, 3082 (1996); **81**, 1774 (1998); A. Aguilar *et al.*, Phys. Rev. D **64**, 112007 (2001).
- [2] A. Aguilar-Arevalo *et al.*, Phys. Rev. Lett. **98**, 231801 (2007).
- [3] H. Pas, S. Pakvasa, and T.J. Weiler, Phys. Rev. D **72**, 095017 (2005).
- [4] G. Karagiorgi, A. Aguilar-Arevalo, J.M. Conrad, M.H. Shaevitz, K. Whisnant, M. Sorel, and V. Barger, Phys. Rev. D **75**, 013011 (2007).
- [5] M. Maltoni and T. Schwetz, Phys. Rev. D **76**, 093005 (2007).
- [6] A.E. Nelson and J. Walsh, Phys. Rev. D **77**, 033001 (2008).
- [7] I.E. Stockdale *et al.*, Phys. Rev. Lett. **52**, 1384 (1984).
- [8] F. Dydak *et al.*, Phys. Lett. B **134**, 281 (1984).
- [9] A. Aguilar-Arevalo *et al.*, Nucl. Instrum. Methods Phys. Res., Sect. A **599**, 28 (2009).
- [10] A. Aguilar-Arevalo *et al.*, Phys. Rev. D **79**, 072002 (2009).
- [11] S. Agostinelli *et al.*, Nucl. Instrum. Methods Phys. Res., Sect. A **506**, 250 (2003).
- [12] M.G. Catanesi *et al.* (HARP Collaboration), Eur. Phys. J. C **52**, 29 (2007).
- [13] I. Chemakin *et al.*, Phys. Rev. C **77**, 015209 (2008); T. Abbott *et al.*, Phys. Rev. D **45**, 3906 (1992); J.V. Allaby *et al.*, Report No. CERN 70-12, 1970; D. Dekkers *et al.*, Phys. Rev. **137**, B962 (1965); G.J. Marmer *et al.*, Phys. Rev. **179**, 1294 (1969); T. Eichten *et al.*, Nucl. Phys. **B44**, 333 (1972); A. Aleshin *et al.*, Report No. ITEP-77-80, 1977; I.A. Vorontsov *et al.*, Report No. ITEP-88-11, 1988.
- [14] CERN Program Library Long Writeup Report No. W5013, 1993.
- [15] D. Casper, Nucl. Phys. B, Proc. Suppl. **112**, 161 (2002).
- [16] A.A. Aguilar-Arevalo *et al.*, Phys. Rev. Lett. **100**, 032301 (2008).
- [17] A. Bodek, S. Avvakumov, R. Bradford, and H. Budd, J. Phys. Conf. Ser. **110**, 082004 (2008).
- [18] X. Espinal and F. Sanchez, AIP Conf. Proc. **967**, 117 (2007).
- [19] R. Gran *et al.*, Phys. Rev. D **74**, 052002 (2006).
- [20] A. Aguilar-Arevalo *et al.*, Phys. Rev. Lett. **102**, 101802 (2009).
- [21] G.J. Feldman and R.D. Cousins, Phys. Rev. D **57**, 3873 (1998).